Specific ion effects on the aggregation behavior of aquatic natural organic matter

Fanchao Xu [a], Yuxuan Yao [a], Pedro J.J. Alvarez [b], Qilin Li [b], Heyun Fu [a], Daqiang Yin [c], Dongqiang Zhu [d], Xiaolei Qu [a,*]

[a] State Key Laboratory of Pollution Control and Resource Reuse, School of the Environment, Nanjing University, Jiangsu 210023, China
[b] Department of Civil and Environmental Engineering, Rice University, Houston, TX 77005, United States
[c] State Key Laboratory of Pollution Control and Resources Reuse, College of Environmental Science and Engineering, Tongji University, Shanghai 200092, China
[d] School of Urban and Environmental Sciences, Peking University, Beijing 100871, China

GRAPHICAL ABSTRACT

ARTICLE INFO

ABSTRACT

Specific ion effects on the aggregation behavior of a reference aquatic natural organic matter (NOM), Suwannee River NOM (SRNOM), were investigated using kinetic, titration, calorimetric, and surface tension methods. Monovalent cations induced structural compacting of SRNOM, but not its aggregation. Their ability to induce structural compacting follows the order: $Cs^+ > Rb^+ > K^+ > Na^+ > Li^+$. Divalent cations except Mg^{2+} can readily induce SRNOM aggregation. Their critical coagulation concentrations (CCC) follow the order: $CCC_{Sr} > CCC_{Ca} > CCC_{Ba}$. Electrokinetic, titration, and calorimetric data suggest that monovalent cations have weak interactions with SRNOM, while divalent cations strongly interact with SRNOM. Overall, the cation specificity in aggregation is determined by cation-NOM interactions and their ability to modulate surface tension. Specific ion effects of monovalent cations correlate to their hydration free energy, while that of divalent cations correlate to the ratio of the hydration entropy of cation to the enthalpy change of cation-NOM interactions. The cation specificity is consistent with the extended Derjaguin-Landau-Verwey-Overbeek theory, and the intermolecular interaction energy is dominated

by the Lewis acid-base interactions. Our results suggest that specific cations should be targeted to predict or manipulate intermolecular interactions of aquatic NOM in natural and engineered settings.

1. Introduction

Natural organic matter (NOM) is a complex mixture of decomposition products of plant and animal residues as well as substances synthesized biologically and/or chemically from these products [1]. Its intermolecular interactions and subsequent aggregation/adsorption processes are key to many important geochemical and engineered processes. The aggregation process converts soluble NOM molecules into particles in aquatic systems, playing an important role in the cycling and export of carbon and other compositional elements [2–4]. The intermolecular interactions of NOM also influence the environmental fate of priority pollutants [5–8] as well as the performance of many water treatment unit processes, especially filtration systems [9,10].

Specific ion effects (i.e., the Hofmeister effects) are of great significance for understanding the interfacial phenomena of particles/macromolecules [11], such as protein-protein interactions and the subsequent aggregation and adsorption processes [12–16]. These phenomena are initially explained by the theory of structure-making ions (kosmotropes) and structure-breaking ions (chaotropes) which affect water structure in different ways and consequently influence the solubility or aggregation behavior of particles/macromolecules. This model was later found flawed as the surface chemistry of particles/macromolecules was not taken into consideration and new evidences suggested no long-range water ordering induced by ions [17]. In a contemporary view, the Hofmeister effects are explained based on direct interactions between ions and particles/macromolecules or their adjacent hydration shell [13,16–18]. The Hofmeister effects of proteins were influenced by the interactions between ions and their peptide backbones as well as surface functional groups (e.g., amide and carboxylate) [17,19,20]. It follows direct or inverse Hofmeister series depending on the sign and density of surface charge, the hydrophobicity and functional groups of the protein surface, and the salt concentration [12,13,16]. In addition, the Hofmeister effects of charged colloidal particles were found to be determined by the valence of ions and ability of ions to interact with particle surfaces [21–23].

Previous studies examined the intermolecular interactions of NOM in the presence of a few naturally abundant cations including Na^+, Mg^{2+}, Ca^{2+}, and Ba^{2+} [9,24–33]. NOM readily forms aggregates in the presence of Ca^{2+} and Ba^{2+} [24–28,30], but not in the presence of Na^+ and Mg^{2+} [26,30]. Ca^{2+} was reported to form bidentate or monodentate inner-sphere coordination with carboxylic groups in NOM [25,26,34]. The strong Ca^{2+}-NOM interactions lead to bridging effect and reduced electrostatic repulsion, facilitating NOM aggregation [9,26,27,30]. Molecular dynamic simulations suggest that Na^+ and Mg^{2+} are not able to induce NOM aggregation [26]. Consistently, Ca^{2+} was reported to induce much stronger fouling of membrane system by humic acids than Mg^{2+} [35]. Mg^{2+} has very limited impacts on the adhesion force between NOM and NOM-fouled membranes as measured by atomic force microscopy [9]. Nevertheless, little is known regarding the aggregation behavior of NOM, a naturally abundant supermolcule, in the context of Hofmeister ordering. Furthermore, the thermodynamic aspects of these specific ion effects are still not clear, which hinders our mechanistic understanding of NOM aggregation.

In the present study, we investigate the aggregation kinetics and thermodynamics of a reference aquatic NOM, Suwannee River NOM (SRNOM), in the presence of nine monovalent and divalent cations. The initial aggregation kinetics of SRNOM was determined using time-resolved dynamic light scattering (*t*-DLS). The cation-SRNOM interactions were examined using electrokinetic, titration, and calorimetric methods. The interaction energies between SRNOM molecules in various solution chemistry were calculated within the framework of the extended Derjaguin-Landau-Verwey-Overbeek (XDLVO) theory in combination of electrokinetic and surface tension measurements. Then, correlations were explored between the SRNOM colloidal behavior and physico-chemical properties of cations. Overall, this effort elucidates the cation specificity for the intermolecular interactions of NOM and the underlying mechanisms in the context of Hofmeister ordering for the first time, which helps understand the significance of Hofmeister phenomenon from environmental perspectives.

2. Materials and methods

2.1. Materials

All chemicals including calcium chloride dihydrate (>99%), lithium chloride (>99%), sodium chloride (>99.5%), rubidium chloride (>99%), cesium chloride ($\geq$99%), magnesium chloride (>99.5%), strontium chloride hexahydrate (>99%), barium chloride dihydrate (>99%), potassium chloride (>99%), hydrochloric acid, and tris (hydroxymethyl) aminomethane ($\geq$99%) were used as received. SRNOM sample (2R101N) was provided by the International Humic Substances Society (IHSS, St. Paul, USA). The elemental composition and acidic functional groups of SRNOM can be found in Table S1. Deionized water (18.2 MΩ·cm resistivity at 25 °C) produced by an ELGA Labwater system (PURELAB Ultra, ELGA Lab-Water Global Operations, UK) was used for all the experiments. The 100 mg/L SRNOM stock solution was prepared by dissolving SRNOM powder in deionized water with pH adjusted to 6.8.

2.2. Aggregation kinetic measurements

The experimental conditions for the measurements mentioned below can be found in Table S2. The aggregation kinetics of SRNOM was determined in various solution chemistry by *t*-DLS measurements using a ZEN 3500 Zetasizer Nano ZS (Malvern, Worcestershire, UK) equipped with a 532-nm laser. The SRNOM stock solution was sonicated in a sonication bath (KH-800TDB, Kunshan Hechuang Ultrasonic Instrument, China) at 50 W for 5 min before the kinetic measurements. In the measurements, 0.2 mL of 100 mg/L SRNOM solution and pre-determined amounts of electrolyte stock solution and deionized water were introduced into a disposable polystyrene cuvette (Sarstedt, Germany) to make a sample with a total volume of 1 mL and SRNOM concentration of 20 mg/L. The NOM concentration is within the range of that found in natural waters. The sample was briefly mixed and immediately analyzed at 25 °C. The *t*-DLS measurements monitor the intensity weighted average hydrodynamic diameter, $d_h(t)$, of SRNOM as a function of time. The autocorrelation function was applied to data collected every 7 s. Note that the hydrolysis of the cations is negligible in the tested conditions.

The initial aggregation rate of SRNOM was determined by applying linear least square regression to the $d_h(t)$ data from the initial value $d_h(0)$ to 1.5 $d_h(0)$. The attachment efficiency, α, is a

key parameter to quantify the tendency of particle aggregation in given water chemistry. It was determined by normalizing the initial aggregation rate in the solution of interest by that in the diffusion-limited regime [36,37]. Stability curves of SRNOM were constructed by plotting the α value as a function of the electrolyte concentration. The initial aggregation rate in the diffusion-limited regime was determined by averaging the initial aggregation rates at the plateau of the stability curve. The critical coagulation concentration (CCC) was determined by the electrolyte concentration where the diffusion-limited regime was achieved. Details about the data analysis and the determination of α and CCC can be found in the supporting information (SI).

2.3. Electrokinetic measurements

The ζ-potential of SRNOM was measured by phase analysis light scattering (PALS) using the ZEN 3500 Zetasizer Nano ZS (Malvern, Worcestershire, UK). Measurements were carried out using disposable folded capillary cells (Malvern, Worcestershire, UK) and five measurements were made for each sample. All ζ-potential measurements were conducted at 25 °C. To explore the responses of SRNOM surface potential to the electrolytes, 0.4 mL of 100 mg/L SRNOM solution and pre-determined amounts of electrolyte stock solution and deionized water were mixed to make a sample with a total volume of 2 mL and SRNOM concentration of 20 mg/L. One milliliter of the sample was introduced into a disposable folded capillary cells (Malvern, Worcestershire, UK) and analyzed by Zetasizer Nano ZS. The concentration range of the electrolyte stock solution was set from 1 mM to 800 mM.

2.4. Titration experiments

The release of H$^+$ during the cation-NOM interaction was measured using titration experiments. Twenty mg/L SRNOM solution was stirred under nitrogen purge and titrated by different cation solutions at room temperature. The initial pH of the SRNOM and cation solutions were adjusted to 6.8. The pH of the solutions were recorded by a pH meter (FE20, Mettler Toledo, Switzerland) and three measurements were made for each titration.

2.5. Cryo-scanning electron microscopy (Cryo-SEM) measurements

Two microliter solution with 1 g/L SRNOM and 300 mM NaCl or 100 mM CaCl$_2$ was mounted on a copper holder, then the sample was frozen by plunging into liquid nitrogen and immediately transferred under vacuum into the chamber of the cryo-attachment work station (ALLTO2500, GATAN, UK). The holder was raised to −110 °C to sublime water and later coated with gold at temperature <−160 °C. After coating, the holder was transferred into the Field Emission SEM (JSM-7800F, JEOL, Japan). The working distance between the stage and the lens was 10 mm. The samples were examined at a low accelerating voltage (3 kV) and the stage temperature of −160 °C.

2.6. Isothermal titration calorimetry measurements

The binding interactions between SRNOM and cations were also investigated using an ITC-200 calorimeter (MicroCal Co., USA). The concentrations of SRNOM and cation solutions were 100 mg/L and 20 mM in Tris-HCl buffer (10 mM, pH 6.8), respectively. All solutions were degassed for 20 min under vacuum before the titration. Experiments were conducted at 25 °C under magnetic stirring at 750 rpm. For each experiment, there was an initial thermal equilibrium time of 60 s. The cation solutions were titrated into SRNOM solutions in 2 μL (first injection of 0.5 μL) aliquots with a 150 s interval. Reference injections of buffer into SRNOM solution were

performed to measure the heat of dilution for each injection, which was subtracted from the integrated data prior to curve fitting. The data was fitted to a two-site binding model using Origin 8.5, and the free energy change (ΔG, kJ/mol), enthalpy change (ΔH, kJ/mol), and entropy change (-TΔS, kJ/mol) for binding of cations to SRNOM were determined.

2.7. Contact angle measurements

The SRNOM solution with different water chemistry was filtered through a reverse osmosis membrane (Reverse Osmosis CE, GE Osmonics, USA) in a reverse osmosis system (HP4750, Sterlitech, USA) to form a cake layer on the membrane. The SRNOM layer was dried by nitrogen gas under room temperature and then subjected to static contact angle measurements. Static contact angles of probe liquids including water, glycerol, and *n*-decane on the surface of SRNOM layer were measured at least three times at different locations by an optical contact angle measuring device (OCA30, Dataphysics Instruments GmbH, Germany).

2.8. Calculation of the interaction energy of SRNOM in different water chemistry

To better understand the interactions between SRNOM in different water chemistry, the XDLVO theory was applied to calculate the total interaction energy (TOT) as the sum of the London-van der Waals force (LW), the electrostatic force (EDL), and the Lewis acid-base interactions (AB) (Eq. (1)) [30,38–41]:

$$\Phi^{Total} = \Phi^{LW} + \Phi^{EDL} + \Phi^{AB} \tag{1}$$

The London-van der Waals interaction energy (Φ^{LW}) for SRNOM was obtained using Eqs. (2) and (3) [38,40]:

$$\Phi^{LW} = -\frac{A}{6}\left[\frac{2a_p^2}{h^2 + 4a_ph} + \frac{2a_p^2}{h^2 + 4a_ph + 4a_p^2} + \ln\left(\frac{h^2 + 4a_ph}{h^2 + 4a_ph + 4a_p^2}\right)\right] \tag{2}$$

$$A = 24\pi h_o^2\left(\sqrt{r_{DBC}^{LW}} - \sqrt{r_w^{LW}}\right)^2 \tag{3}$$

where A is the Hamaker constant, a_p is the radius of SRNOM particle, h is the separation distance between the surfaces, h_0 represents the minimum equilibrium distance between SRNOM particles and was set to be 0.157 nm, and r_{DBC}^{LW} and r_w^{LW} are the LW interfacial tension parameters for SRNOM and water, respectively.

The electrostatic interaction energy (Φ^{EDL}) for SRNOM was calculated using Eqs. (4) and (5) [39]:

$$\Phi^{EDL} = 2\pi\varepsilon_0\varepsilon_w a_p\psi_p^2\exp(-\kappa h) \tag{4}$$

$$\kappa = \sqrt{\frac{e^2 \sum n_{i0}z_i^2}{\varepsilon_0\varepsilon_w k_B T}} \tag{5}$$

where ε_0 is the dielectric permittivity of vacuum, ε_w is the dielectric constant of water, ψ_p is the ζ-potential of SRNOM particles, κ is the inverse of Debye length, e is the electron charge, n_{i0} and z_i are the number concentration and valence of ion i in the bulk suspension, k_B is the Boltzmann constant, and T is the absolute temperature. Eq. (4) was sufficiently accurate to predict electrostatic interaction energies even in asymmetrical electrolyte solutions (i.e., divalent cation solutions), which are consistent with the direct force measurements [39].

The AB interaction energy (Φ^{AB}) for SRNOM was obtained using Eq. (6) [38,41]:

$$\Phi^{AB} = \pi a_p \lambda_w \Delta G_{h_0}^{AB} \exp\left[\frac{h_0 - h}{\lambda_w}\right] \tag{6}$$

where λ_w is the characteristic decay length of AB interactions in water (1.0 nm at 20 °C) and $\Delta G_{h_0}^{AB}$ represents the Lewis acid-base interaction free energy per unit area corresponding to h_o, and can be obtained using Eq. (7).

The ΔG^{AB} of SRNOM particles in water was calculated using Eq. (7) [38]:

$$\Delta G^{AB} = -4\left(\sqrt{\gamma_i^+ \gamma_i^-} + \sqrt{\gamma_w^+ \gamma_w^-} - \sqrt{\gamma_i^+ \gamma_w^-} - \sqrt{\gamma_w^+ \gamma_i^-}\right) \tag{7}$$

where the subscript i represents SRNOM and w represents water, and γ^+ and γ^- are the electron-acceptor and electron-donor parameters of the polar surface tension component, respectively. For SRNOM, the values of γ_i^+ and γ_i^- can be calculated from measuring the air-liquid-SRNOM contact angles (θ) using three different probe liquids (water, glycerol, and n-decane) with known surface tension parameters and by solving Young-Dupré equation (Eq. (8)) [38]:

$$\gamma_p^{Tot}(1 + \cos\theta) = 2\left(\sqrt{\gamma_i^{LW}\gamma_P^{LW}} + \sqrt{\gamma_p^+ \gamma_i^-} + \sqrt{\gamma_i^+ \gamma_p^-}\right) \tag{8}$$

where the subscript p represents the liquid used for contact angle measurement, including water (γ_w^{Tot} = 72.8, γ_w^{LW} = 21.8, and $\gamma_w^+ = \gamma_w^-$ = 25.5 mJ/m^2), glycerol (γ_g^{Tot} = 64.0, γ_g^{LW} = 34.0, γ_g^+ = 3.92 and γ_g^- = 25.5 mJ/m^2), and n-decane (γ_d^{Tot} = 23.8, γ_d^{LW} = 23.8, $\gamma_d^+ = \gamma_d^-$ = 0 mJ/m^2).

3. Results and discussion

3.1. Interactions between cations and SRNOM

The cation-NOM interactions were examined using electrokientic, titration, and calorimetric methods. The electrokinetic properties of SRNOM were examined over a wide range of monovalent and divalent cation concentrations as summarized in Fig. 1. In monovalent cation solutions, SRNOM became less negatively charged as the salt concentration increased from 1 mM to 800 mM owing to charge screening (Fig. 1a) [30,42]. Note that the high electrolyte concentration used here is to probe the potential charge reversal phenomenon. At any given salt concentration, the ζ-potential of SRNOM follows the order of $|\zeta_{Li}| > |\zeta_{Na}| > |\zeta_K| > |\zeta_{Rb}| > |\zeta_{Cs}|$, consistent with the order of cations in periodic group IA and the hydrated ionic radii (Table S3). The ζ-potential of

SRNOM in divalent cation solutions became less negatively charged as salt concentration increased at low cation concentrations (Fig. 1b). They are more efficient than monovalent cations in reducing the surface potential of SRNOM, consistent with the Schulze-Hardy rule [43]. The ability of divalent cations in reducing the surface potential of SRNOM at a given concentration follows the order of Ba^{2+} > Ca^{2+} > Sr^{2+} > Mg^{2+}. As the salt concentration further increased, the ζ-potential of SRNOM reversed from negative to positive in Ba^{2+}, Ca^{2+}, and Sr^{2+} solutions, but not in Mg^{2+} solutions. The charge reversal concentration, c_R, (i.e., the concentration of electrolyte at the isoelectric point) follows the order of $c_{R(Sr)} > c_{R(Ca)} > c_{R(Ba)}$. The order of Ca and Sr is not consistent with their positions in periodic group IIA. The charge reversal phenomenon cannot be explained by electric double layer models. It was previously linked to formation of adsorbed layer of cationic polyelectrolytes, charge correlation effect, or specific sorption [21,22,44–49]. We postulate that divalent cations, except Mg^{2+}, can strongly interact with SRNOM molecules, leading to the overcharging phenomenon.

Titration and ITC experiments were carried out to further understand the cation-NOM interactions. The amount of H$^+$ released from SRNOM during the titration of cations is summarized in Fig. 2 (titration curves can be found in Fig. S1). Monovalent and divalent cations have quite different H$^+$ exchange patterns. Monovalent cations have low H$^+$ exchange capacity as shown in Fig. 2a. Their H$^+$ exchange capacity follows the order of Cs$^+$ > Rb$^+$ ≫ K$^+$ > Na$^+$, Li$^+$. Divalent cations have higher H$^+$ exchange capacity than monovalent (Fig. 2b). Their H$^+$ exchange capacity follows the order of Ba^{2+} > Ca^{2+} > Sr^{2+} > Mg^{2+}.

The ITC data for the interactions of SRNOM with all the cations can be found in Fig. S2. There was small free energy change during the titration of monovalent solutions into SRNOM solution, indicating weak interactions between these cations and SRNOM. The free energy changes for divalent cations are all significantly negative, suggesting spontaneous cation-NOM interactions (Fig. S2 and thermodynamic parameters including ΔH, ΔS, and ΔG for divalent cation-SRNOM binding can be found in Table S4). For all the divalent cations except Mg^{2+}, their $|\Delta H|$ was higher than $|T\Delta S|$. Thus, the interactions are mainly driven by enthalpy changes, except Mg^{2+}. The enthalpy changes followed the order of ΔH_{Ba} (−83.50 kcal/mol) > ΔH_{Sr} (−2.90 kcal/mol) > ΔH_{Ca} (−2.85 kcal/mol) > ΔH_{Mg} (−81.28 kcal/mol). The negative value of ΔH indicates an exothermic binding reaction [35]. The electrokinetic, titration, and calorimetric data agree with each other well. The interactions
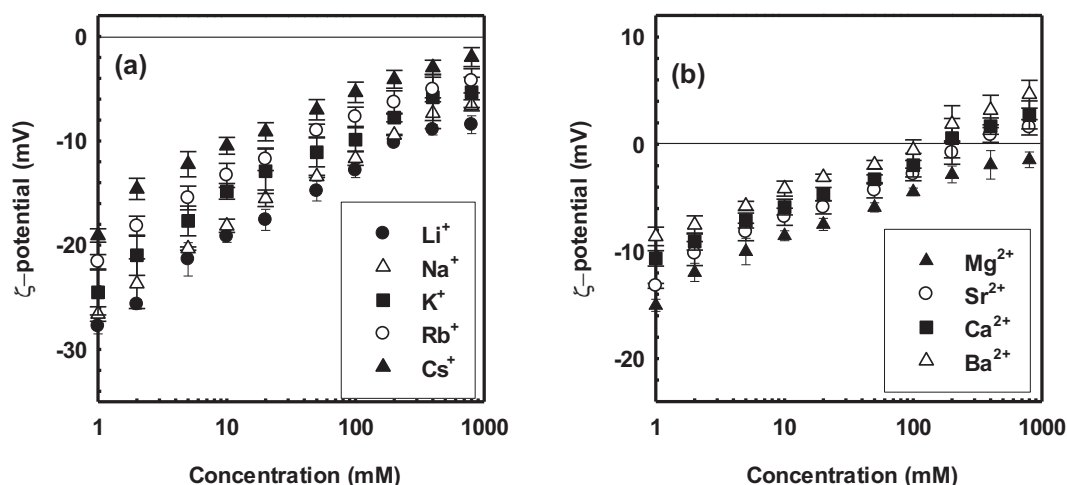

Fig. 1. ζ-potential of SRNOM as a function of (a) monovalent and (b) divalent cation concentration. Error bar represents one standard deviation from the mean of five measurements.
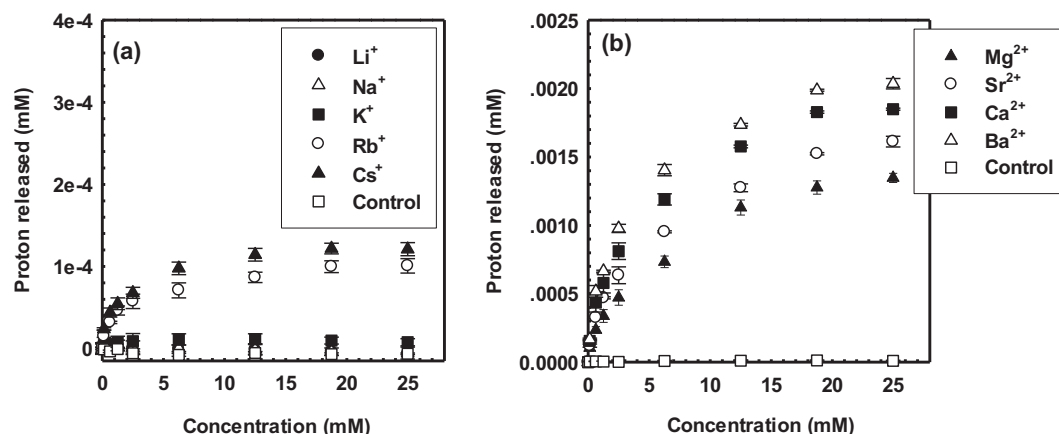
Fig. 2. Proton released during the titration of cations as a function of (a) monovalent and (b) divalent cation concentrations in 20 mg/L SRNOM solutions. Error bar represents one standard deviation from the mean of three measurements.

between monovalent cations and SRNOM are relatively weak. Divalent cations, except Mg^{2+}, can strongly interact with SRNOM, directly altering its surface charge (see more details below).

3.2. Strong specific ion effects on the aggregation behavior of SRNOM

The initial aggregation kinetics of SRNOM in the presence of monovalent and divalent cations is summarized in Fig. 3. The impacts of these cations on the colloidal stability of SRNOM can be divided into two groups: monovalent cations and Mg^{2+} *vs.* other

divalent cations. There was no increase of SRNOM particle size in the presence of 300 mM monovalent cations and 100 mM $MgCl_2$ (the same ionic strength as 300 mM monovalent cation chloride solutions) in 1 h (Fig. 3a and b). A close look at Fig. 3a and b revealed different patterns among these cations. For monovalent cations and Mg^{2+}, the size of SRNOM initially decreased and stabilized afterward. This structural compacting phenomenon was previously observed for NOM and polyelectrolytes [4,30,50,51]. The equilibrium particle diameter (d_e) in different cation solutions follows the order of d_e(Li) > d_e(Na) > d_e(K) > d_e(Rb) > d_e(Cs) > d_e(Mg).
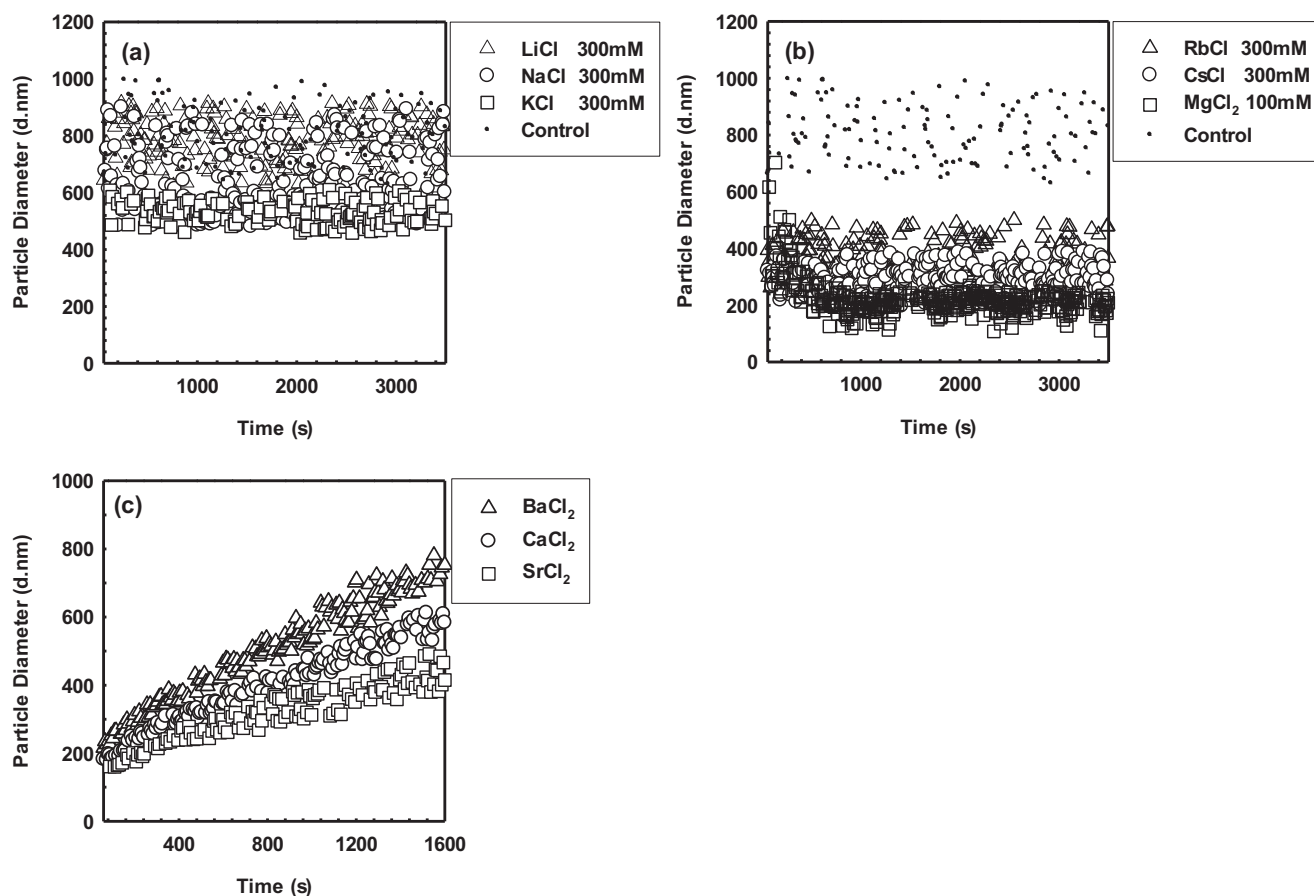

Fig. 3. Initial aggregation profiles of SRNOM in (a) 300 mM LiCl, NaCl, KCl solutions, (b) 300 mM RbCl, CsCl, and 100 mM $MgCl_2$ solution (i.e., the same ionic strength as 300 mM monovalent cation chloride solutions), and in (c) 10 mM different divalent cation solutions at pH 6.4 ± 0.2 measured by time-resolved dynamic light scattering.

On the other hand, 10 mM $CaCl_2$, $SrCl_2$, and $BaCl_2$ can induce significant aggregation of SRNOM as shown in Fig. 3c. The particle size did not reach equilibrium in these electrolyte solutions in the test period. At the given salt concentration (i.e., 10 mM), the initial aggregation rate (r) increases as $r_{Sr} < r_{Ca} < r_{Ba}$ (Fig. 3c). The aggregation data were generally consistent with the cryo-SEM micrographs (Fig. S3). In 300 mM NaCl solution, SRNOM presented as irregular shapes with sizes in the sub-μm to μm range. In 100 mM $CaCl_2$ solution (the same ionic strength of 300 mM NaCl), SRNOM formed large network structures, consistent with previous findings [32].

For divalent cations able to induce aggregation, the attachment efficiency, α, of SRNOM was determined as a function of salt concentration (Fig. 4). The attachment efficiency, scaling from 0 to 1, represents the probability of successful attachment during a collision event in given water chemistry. The stability plots of all cations contain two distinct regimes. The attachment efficiency initially increases with salt concentration, which is usually referred to as reaction-limited regime. Then it reaches a plateau at unity as the salt concentration exceeds the critical coagulation concentration (CCC), where the aggregation is controlled solely by the diffusion process (i.e., diffusion-limited regime). The CCC follows the order of $CCC_{Sr} > CCC_{Ca} > CCC_{Ba}$ (Fig. 4). These results suggest strong cation specificity for the aggregation of SRNOM. If assume the aggregation of SRNOM was controlled by DLVO forces (i.e., London-van der Waals force and electrostatic force), the critical coagulation ionic strength (CCIS) will depend on the ζ-potential [52]:

$$CCIS \propto \zeta^4 \tag{9}$$

Our data suggest that for SRNOM the $CCIS \propto \zeta^{1.8}$ (Fig. S4), indicating that additional force needs to be considered.

3.3. Interaction energies of SRNOM in electrolyte solutions

The interaction energies of London-van der Waals force, electrostatic force, Lewis acid-base interactions, and the total interaction energy of SRNOM in electrolyte solutions were calculated in the framework of XDLVO theory to better understand the observed specific ion effects [30,38]. The contact angle measurements, surface tension components, Hamaker constant, and the Lewis acid-base interaction free energy ($\Delta G_{h_0}^{AB}$) for SRNOM in different water chemistry can be found in Tables S5 and S6. The energy profiles of SRNOM in 30 mM monovalent cation solutions are summarized
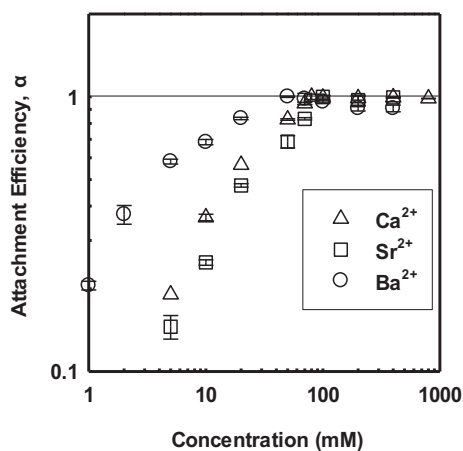

Fig. 4. Attachment efficiency of SRNOM as a function of $CaCl_2$, $SrCl_2$, and $BaCl_2$ concentration. Error bar represents one standard deviation from the mean of triplicate measurements.

in Fig. S5 and their total interaction energies summarized in Fig. 5a. The Debye length of SRNOM is calculated to be 1.74 nm. Repulsive Lewis-acid-base interactions (i.e., hydration force) became significant (>1 k_BT) at distance of 6–7 nm, which is farther than the electrostatic force in the corresponding electrolyte solution (Table S7) and the Debye length. Thus, the approaching SRNOM particles experience significant hydration force first. Meanwhile, the interaction energies of Lewis acid-base interactions are orders of magnitudes higher than that of electrostatic force (Fig. S5). As a result, Lewis-acid-base interactions are more important than the electrostatic force in terms of both interaction range and strength. The strong hydration force is consistent with the hydrophilic nature of SRNOM, which leads to high energy barrier for the attachments of SRNOM molecules [38,53]. High energy barrier (>1465.4 k_BT) stabilized SRNOM molecules, leading to the minimal aggregation of SRNOM in monovalent cation solutions (Fig. 5a). The energy barrier decreases with the order of cations in periodic group IA from 1663.8 k_BT (Li^+) to 1465.4 k_BT (Cs^+). They are positively correlated to the equilibrium particle diameter (d_e) of SRNOM in different cation solutions (Fig. 5b).

The total interaction energies of SRNOM in 10 mM divalent cation solutions are summarized in Fig. 6a (See detailed energy profiles of SRNOM in divalent cation solutions in Fig. S6). The energy barrier in 10 mM Mg^{2+} solution is 1090.9 k_BT, which is much lower than that in 30 mM monovalent cation solutions (1465.4–1663.8 k_BT). Nevertheless, it's still high enough to stabilize SRNOM molecules. The energy barriers in 10 mM Ba^{2+}, Ca^{2+}, and Sr^{2+} solutions are 71.1 k_BT, 270.0 k_BT, and 367.7 k_BT, respectively. Thus, SRNOM aggregation was observed in these solutions (Fig. 3c). The energy barriers are inversely correlated to the attachment efficiencies of SRNOM in different cation solutions (Fig. 6b). These results suggest that the aggregation behavior of SRNOM can be decently described by the XDLVO theory.

3.4. Correlations between the NOM colloidal behavior and physicochemical properties of cations

Correlations between colloidal behavior of SRNOM and physicochemical properties of cations and the underlying mechanisms were further explored (Figs. 7 and 8). For monovalent cations, the equilibrium particle diameter of SRNOM (d_e) was chosen as the colloidal behavior index. SRNOM has abundant carboxyl (11.21 meq/g C) and phenolic (2.47 meq/g C) groups (Table S1), providing electrostatic repulsion between functional groups and resulting in stretched configurations [56–58]. Monovalent cations can reduce the intramolecular electrostatic repulsion, leading to a more compact configuration. Monovalent cations with small ionic radii are highly hydrated in aqueous solution (see the ionic and hydrated radii of all the cations tested in Table S3). They generally have weak influence on the Lewis-acid-base interactions, consistent with the XDLVO calculations and a previous study [30]. But monovalent cations with lower hydration free energy (e.g., $Cs^+ < Rb^+ < K^+ < Na^+ < Li^+$) has higher ability to induce cation-NOM interactions as suggested by the electrokinetic, titration, and ITC data and they are consequently more effective in reducing hydration force. This agrees with a previous study which suggests that Cs^+ can form outer-sphere complexes with NOM [59]. Thus, there is a strong linear correlation between d_e and hydration free energy of mono-valent cation as shown in Fig. 7.

For divalent cations, the CCC was chose as the colloidal behavior index. They have stronger interactions with SRNOM than monovalent cations as suggested by electrokinetic, titration, and ITC data. Mg^{2+} behaves differently from other divalent cations and cannot induce significant aggregation and charge reversal of SRNOM, indicating that the direct interactions between Mg^{2+} and SRNOM are moderate [26,30,60]. This agrees with a previous study which
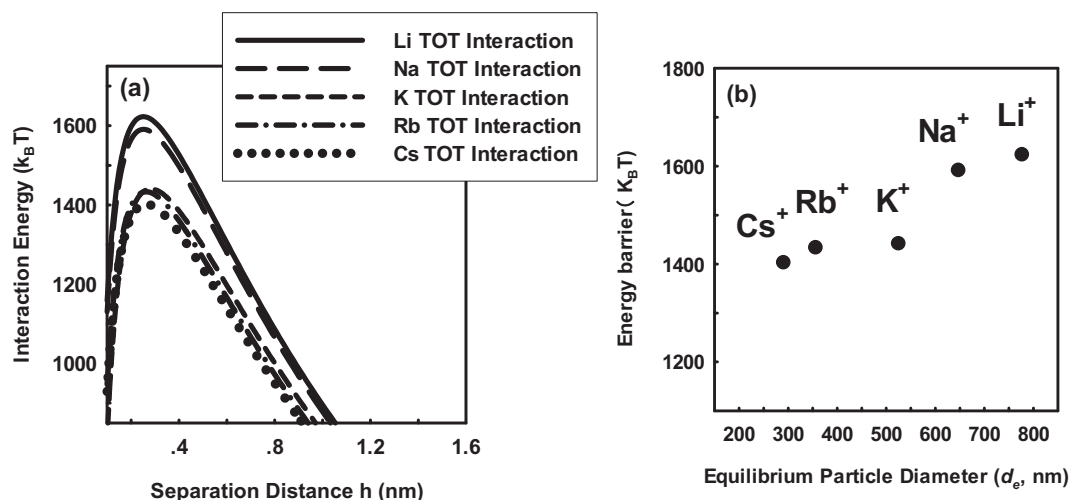
Fig. 5. (a) The total interaction energy (TOT) of SRNOM in 30 mM monovalent cation solutions; (b) the correlation between the energy barriers of SRNOM in 30 mM monovalent cation solutions and the equilibrium particle diameter (d_e).
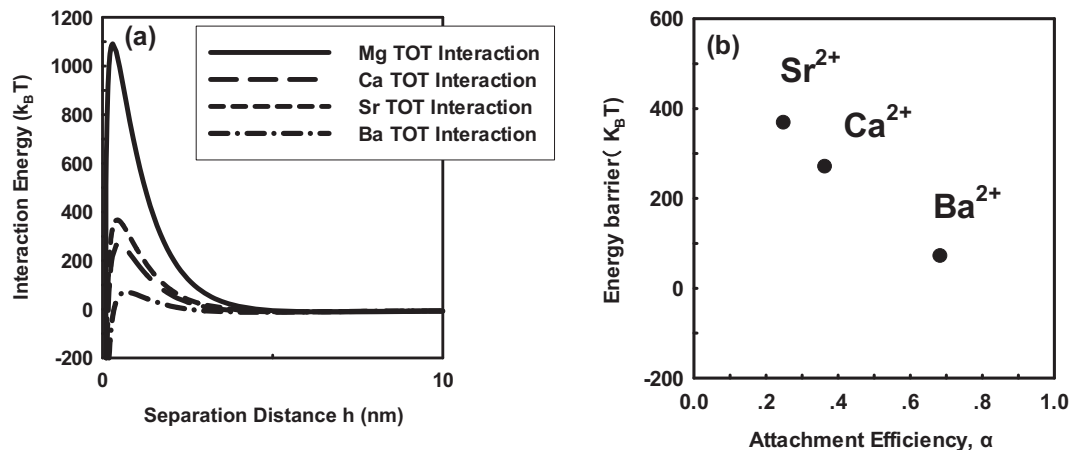

Fig. 6. (a) The total interaction energy (TOT) of SRNOM in 10 mM divalent cation solutions; (b) the correlation between the energy barriers of SRNOM in 10 mM divalent cation solutions and the attachment efficiency, α.
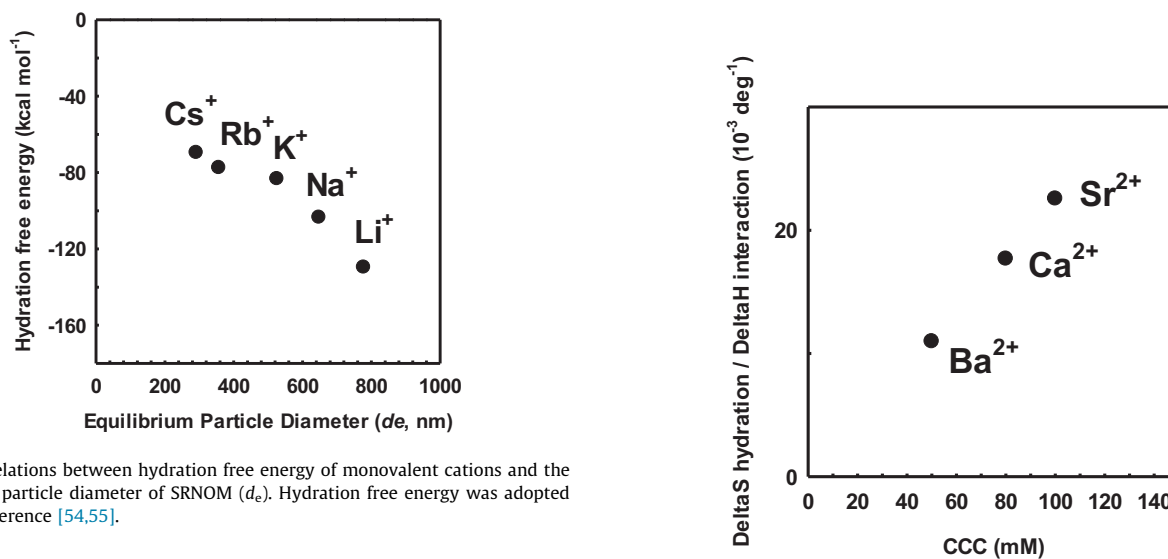

Fig. 7. Correlations between hydration free energy of monovalent cations and the equilibrium particle diameter of SRNOM (d_e). Hydration free energy was adopted from the reference [54,55].

suggest Mg^{2+} does not bind strongly to NOM due to its well defined second hydration shell [60]. Consistently, Mg^{2+} has the lowest H^+ exchange capacity and $\Delta H_{interaction}$ in all divalent cations (Fig. 2b,

Fig. 8. Correlation between $\Delta S_{hydration}/\Delta H_{interaction}$ of divalent cations and the critical coagulation concentration (CCC) of SRNOM in the corresponding cation solutions. $\Delta S_{hydration}$ values were adopted from the reference [54].

Table S3). Other divalent cations can strongly interact with SRNOM through outer-sphere or partially inner-sphere complexation mechanisms [25,26,34]. These direct interactions significantly reduce the surface charge (Fig. 1) and more importantly the Lewis acid-base interactions of SRNOM molecules, leading to lower energy barrier (Fig. 6). In some conditions, the Lewis acid-base interactions even shift from repulsive (i.e., hydration force) to attractive (i.e., hydrophobic effect). For example, the ΔG^{AB} of SRNOM decreased from 8.8 to -3.1 mJ m^{-2} as CaCl$_2$ concentration increased from 10 to 100 mM. This is because that the bonded cations neutralize the charge of SRNOM molecules and shield the polar groups, leaving more hydrocarbon structures exposed to the water phase [61]. In terms of surface tension, divalent cations significantly reduces the electron-donor surface tension component (γ^-) and increases electron-acceptor surface tension component (γ^+) of SRNOM (Table S6). In addition, divalent cations can potentially bridge the carboxyl groups in different SRNOM molecules, resulting bridging effect which facilitates aggregation [24]. The ability of a cation to induce SRNOM aggregation is determined by the ability of the cation to interact with NOM and its immediate hydration shell. The binding enthalpy ($\Delta H_{\text{interaction}}$) can reflect the strength of the interactions between NOM and cations [62]. The hydration entropy ($\Delta S_{\text{hydration}}$) of ions can reflect the state of its hydration shell, which was previously found to correlated well the Hofmeister effects [13]. Thus, we chose $\Delta H_{\text{interaction}}$ to quantify the cation-NOM interactions and $\Delta S_{\text{hydration}}$ to quantify the hydration states of cations. The CCC of SRNOM in different divalent cation solutions increases linearly with $\Delta S_{\text{hydration}}/\Delta H_{\text{interaction}}$ (Fig. 8).

4. Conclusion

This study systematically reveals the Hofmeister phenomenon in the colloidal behavior of NOM for the first time. It suggests that our understanding of Hoffmeister phenomenon can be applied to the aggregation behavior of NOM. We found that the colloidal stability of aquatic NOM was mainly determined by the Lewis acid-base interactions of NOM molecules. The ability of cations to induce NOM aggregation was determined by cation-NOM interactions and their ability to modulate surface tension. Thus, the aggregation and attachment of NOM molecules in aquatic systems are significantly influenced by some specific cations such as Ca^{2+}, Sr^{2+}, and Ba^{2+}. Many naturally abundant cations, including Na$^+$ and K$^+$, have limited influence on these processes. It indicates that the concentrations of cations that can strongly interact with NOM need to be determined for accurate prediction of NOM intermolecular interactions, in addition to general measurements of ion concentrations (e.g., conductivity). In engineered systems where strong intermolecular interactions of NOM are detrimental (e.g., organic fouling of membrane systems or saturation of adsorption capacity), NOM hydrophobicity in the source water is a key parameter for the treatment performance. The structural diversity of NOM was not considered in this study. Future research is needed to address the relationships between NOM structure and its interfacial behavior within the context of specific ion effects. There are also great needs in developing convenient techniques for the quantification of NOM hydrophobicity.

Acknowledgements

Appendix A. Supplementary material

Supplementary data to this article can be found online at https://doi.org/10.1016/j.jcis.2019.09.001.

References

[1] G.R. Aiken, Humic substances in soil, sediment, and water: geochemistry, isolation, and characterization (1985).
[2] A. Engel, S. Thoms, U. Riebesell, E. Rochelle-Newall, I. Zondervan, Polysaccharide aggregation as a potential sink of marine dissolved organic carbon, Nature 428 (6986) (2004) 929–932.
[3] C.S. Hopkinson, J.J. Vallino, Efficient export of carbon to the deep ocean through dissolved organic matter, Nature 433 (7022) (2005) 142–145.
[4] W.C. Chin, M.V. Orellana, P. Verdugo, Spontaneous assembly of marine dissolved organic matter into polymer gels, Nature 391 (6667) (1998) 568–572.
[5] M.A. Schlautman, J.J. Morgan, Effects of aqueous chemistry on the binding of polycyclic aromatic-hydrocarbons by dissolved humic materials, Environ. Sci. Technol. 27 (5) (1993) 961–969.
[6] H. Fu, C. Wei, X. Qu, H. Li, D. Zhu, Strong binding of apolar hydrophobic organic contaminants by dissolved black carbon released from biochar: a mechanism of pseudomicelle partition and environmental implications, Environ. Pollut. 232 (2018) 402–410.
[7] F.D. Kopinke, A. Georgi, K. MacKenzie, Sorption of pyrene to dissolved humic substances and related model polymers. 1. Structure-property correlation, Environ. Sci. Technol. 35 (12) (2001) 2536–2542.
[8] Y.K. Mouvenchery, J. Kučerík, D. Diehl, G.E. Schaumann, Cation-mediated cross-linking in natural organic matter: a review, Rev. Environ. Sci. Bio. 11 (1) (2012) 41–54.
[9] Q. Li, M. Elimelech, Organic fouling and chemical cleaning of nanofiltration membranes: measurements and mechanisms, Environ. Sci. Technol. 38 (17) (2004) 4683–4693.
[10] S. Lee, M. Elimelech, Relating organic fouling of reverse osmosis membranes to intermolecular adhesion forces, Environ. Sci. Technol. 40 (3) (2006) 980–987.
[11] M.G. Cacace, E.M. Landau, J.J. Ramsden, The Hofmeister series: salt and solvent effects on interfacial phenomena, Q. Rev. Biophys. 30 (3) (1997) 241–277.
[12] Y. Zhang, P.S. Cremer, The inverse and direct Hofmeister series for lysozyme, Proc. Natl. Acad. Sci. U.S.A. 106 (36) (2009) 15249–15253.
[13] Y.J. Zhang, P.S. Cremer, Interactions between macromolecules and ions: the Hofmeister series, Curr. Opin. Chem. Biol. 10 (6) (2006) 658–663.
[14] K.D. Collins, Ions from the Hofmeister series and osmolytes: effects on proteins in solution and in the crystallization process, Methods 34 (3) (2004) 300–311.
[15] D. Constantinescu, H. Weingartner, C. Herrmann, Protein denaturation by ionic liquids and the Hofmeister series: A case study of aqueous solutions of ribonuclease A, Angew. Chem. Int. Edit. 46 (46) (2007) 8887–8889.
[16] N. Schwierz, D. Horinek, U. Sivan, R.R. Netz, Reversed Hofmeister series—The rule rather than the exception, Curr. Opin. Colloid In. 23 (2016) 10–18.
[17] P. Jungwirth, P.S. Cremer, Beyond Hofmeister, Nat. Chem. 6 (4) (2014) 261–263.
[18] P.S. Cremer, A.H. Flood, B.C. Gibb, D.L. Mobley, Collaborative routes to clarifying the murky waters of aqueous supramolecular chemistry, Nat. Chem. 10 (2017) 8.
[19] J. Paterová, K.B. Rembert, J. Heyda, Y. Kurra, H.I. Okur, W.R. Liu, C. Hilty, P.S. Cremer, P. Jungwirth, Reversal of the Hofmeister Series: specific ion effects on peptides, J. Phys. Chem. B 117 (27) (2013) 8150–8158.
[20] H.I. Okur, J. Kherb, P.S. Cremer, Cations bind only weakly to amides in aqueous solutions, J. Am. Chem. Soc. 135 (13) (2013) 5062–5067.
[21] T. Oncsik, G. Trefalt, Z. Csendes, I. Szilagyi, M. Borkovec, Aggregation of negatively charged colloidal particles in the presence of multivalent cations, Langmuir 30 (3) (2014) 733–741.
[22] T. Oncsik, G. Trefalt, M. Borkovec, I. Szilagyi, Specific ion effects on particle aggregation induced by monovalent salts within the Hofmeister Series, Langmuir 31 (13) (2015) 3799–3807.
[23] S. Muráth, S. Sáringer, Z. Somosi, I. Szilágyi, Effect of ionic compounds of different valences on the stability of titanium oxide colloids, Colloids Interf. 2 (3) (2018) 32.
[24] N. Kloster, M. Brigante, G. Zanini, M. Avena, Aggregation kinetics of humic acids in the presence of calcium ions, Colloids Surf. A 427 (2013) 76–82.
[25] A.G. Kalinichev, E. Iskrenova-Tchoukova, W.Y. Ahn, M.M. Clark, R.J. Kirkpatrick, Effects of Ca^{2+} on supramolecular aggregation of natural organic matter in aqueous solutions: a comparison of molecular modeling approaches, Geoderma 169 (2011) 27–32.
[26] E. Iskrenova-Tchoukova, A.G. Kalinichev, R.J. Kirkpatrick, Metal cation complexation with natural organic matter in aqueous solutions: molecular dynamics simulations and potentials of mean force, Langmuir 26 (20) (2010) 15909–15919.
[27] M. Terashima, S. Tanaka, M. Fukushima, Coagulation characteristics of humic acid modified with glucosamine or taurine, Chemosphere 69 (2) (2007) 240–246.

[28] N.A. Wall, G.R. Choppin, Humic acids coagulation: influence of divalent cations, Appl. Geochem. 18 (10) (2003) 1573–1582.
[29] I. Christl, R. Kretzschmar, C-1s NEXAFS Spectroscopy reveals chemical fractionation of humic acid by cation-induced coagulation, Environ. Sci. Technol. 41 (6) (2007) 1915–1920.
[30] F. Xu, C. Wei, Q. Zeng, X. Li, P.J.J. Alvarez, Q. Li, X. Qu, D. Zhu, Aggregation behavior of dissolved black carbon: implications for vertical mass flux and fractionation in aquatic systems, Environ. Sci. Technol. 51 (23) (2017) 13723–13732.
[31] R.R. Engebretson, R. von Wandruszka, Kinetic Aspects of cation-enhanced aggregation in aqueous humic acids, Environ. Sci. Technol. 32 (4) (1998) 488–493.
[32] M. Baalousha, M. Motelica-Heino, P.L. Coustumer, Conformation and size of humic substances: effects of major cation concentration and type, pH, salinity, and residence time, Colloids Surf. A 272 (1) (2006) 48–55.
[33] S. Tamamura, R. Ohashi, S. Nagao, M. Yamamoto, M. Mizuno, Molecular-size-distribution-dependent aggregation of humic substances by Na(I), Ag(I), Ca(II), and Eu(III), Colloids Surf. A 434 (2013) 9–15.
[34] R. Sutton, G. Sposito, M.S. Diallo, H.R. Schulten, Molecular simulation of a model of dissolved organic matter, Environ. Toxicol. Chem. 24 (8) (2005) 1902–1911.
[35] L.F. Wang, D.Q. He, W. Chen, H.Q. Yu, Probing the roles of Ca^{2+} and Mg^{2+} in humic acids-induced ultrafiltration membrane fouling using an integrated approach, Water Res. 81 (2015) 325–332.
[36] K.L. Chen, M. Elimelech, Aggregation and deposition kinetics of fullerene (C_{60}) nanoparticles, Langmuir 22 (26) (2006) 10994–11001.
[37] X. Qu, Y.S. Hwang, P.J.J. Alvarez, D. Bouchard, Q. Li, UV Irradiation and humic acid mediate aggregation of aqueous fullerene (nC_{60}) nanoparticles, Environ. Sci. Technol. 44 (20) (2010) 7821–7826.
[38] C.J. Van Oss, Hydrophobicity of biosurfaces—Origin, quantitative determination and interaction energies, Colloids Surf. B 5 (3–4) (1995) 91–110.
[39] P. Sinha, I. Szilagyi, F.J. Montes Ruiz-Cabello, P. Maroni, M. Borkovec, Attractive forces between charged colloidal particles induced by multivalent ions revealed by confronting aggregation and direct force measurements, J. Phys. Chem. Lett. 4 (4) (2013) 648–652.
[40] Y. Zhang, Y.S. Chen, P. Westerhoff, K. Hristovski, J.C. Crittenden, Stability of commercial metal oxide nanoparticles in water, Water Res. 42 (8–9) (2008) 2204–2212.
[41] D.J. Wang, W. Zhang, X.Z. Hao, D.M. Zhou, Transport of biochar particles in saturated granular media: effects of pyrolysis temperature and particle size, Environ. Sci. Technol. 47 (2) (2013) 821–828.
[42] L.F. Wang, L.L. Wang, X.D. Ye, W.W. Li, X.M. Ren, G.P. Sheng, H.Q. Yu, X.K. Wang, Coagulation kinetics of humic aggregates in mono- and di-valent electrolyte solutions, Environ. Sci. Technol. 47 (10) (2013) 5042–5049.
[43] W.B. Hardy, A preliminary investigation of the conditions which determine the stability of irreversible hydrosols, Proc. Ro. Soc. London 66 (426) (1900) 110–125.
[44] K. Besteman, K. Van Eijk, S.G. Lemay, Charge inversion accompanies DNA condensation by multivalent ions, Nat. Phys. 3 (9) (2007) 641–644.
[45] J. Hierrezuelo, A. Vaccaro, M. Borkovec, Stability of negatively charged latex particles in the presence of a strong cationic polyelectrolyte at elevated ionic strengths, J. Colloid Interf. Sci. 347 (2) (2010) 202–208.
[46] I. Szilagyi, A. Polomska, D. Citherlet, A. Sadeghpour, M. Borkovec, Charging and aggregation of negatively charged colloidal latex particles in the presence of multivalent oligoamine cations, J. Colloid Interf. Sci. 392 (2013) 34–41.
[47] C. Schneider, M. Hanisch, B. Wedel, A. Jusufi, M. Ballauff, Experimental study of electrostatically stabilized colloidal particles: colloidal stability and charge reversal, J. Colloid Interf. Sci. 358 (1) (2011) 62–67.
[48] J. Lyklema, Overcharging, charge reversal: Chemistry or physics?, Colloids Surf A 291 (1–3) (2006) 3–12.
[49] M. Borkovec, I. Szilagyi, I. Popa, M. Finessi, P. Sinha, P. Maroni, G. Papastavrou, Investigating forces between charged particles in the presence of oppositely charged polyelectrolytes with the multi-particle colloidal probe technique, Adv. Colloid Interf. 179–182 (2012) 85–98.
[50] R.R. Engebretson, T. Amos, R. von Wandruszka, Quantitative approach to humic acid associations, Environ. Sci. Technol. 30 (3) (1996) 990–997.
[51] P.Y. Hsiao, E. Luijten, Salt-induced collapse and reexpansion of highly charged flexible polyelectrolytes, Phys. Rev. Lett. 97 (14) (2006) 148301.
[52] G. Trefalt, I. Szilagyi, G. Téllez, M. Borkovec, Colloidal stability in asymmetric electrolytes: modifications of the Schulze-Hardy Rule, Langmuir 33 (7) (2017) 1695–1704.
[53] C.J. van Oss, Acid—base interfacial interactions in aqueous media, Colloids Surf. A 78 (Supplement C) (1993) 1–49.
[54] R.M. Noyes, Thermodynamics of ion hydration as a measure of effective dielectric properties of water, J. Am. Chem. Soc. 84 (4) (1962) 513–522.
[55] A. Voet, Quantitative lyotropy, Chem. Rev. 20 (2) (1937) 169–179.
[56] M.N. Tamashiro, H. Schiessel, Stepwise unwinding of polyelectrolytes under stretching, Macromolecules 33 (14) (2000) 5263–5272.
[57] S.G. Wang, X.F. Sun, X.W. Liu, W.X. Gong, B.Y. Gao, N. Bao, Chitosan hydrogel beads for fulvic acid adsorption: behaviors and mechanisms, Chem. Eng. J. 142 (3) (2008) 239–247.
[58] C. Dong, W. Chen, C. Liu, Y. Liu, H. Liu, Synthesis of magnetic chitosan nanoparticle and its adsorption property for humic acid from aqueous solution, Colloids Surf. A (2014) 179–189.
[59] X. Xu, A.G. Kalinichev, R. James Kirkpatrick, ^{133}Cs and ^{35}Cl NMR spectroscopy and molecular dynamics modeling of Cs^+ and Cl^- complexation with natural organic matter, Geochim. Cosmochim. Ac. 70 (17) (2006) 4319–4331.
[60] A.G. Kalinichev, R.J. Kirkpatrick, Molecular dynamics simulation of cationic complexation with natural organic matter, Eur. J. Soil Sci. 58 (4) (2007) 909–917.
[61] S. Ohki, A mechanism of divalent ion-induced phosphatidylserine membrane fusion, BBA-Biomembranes 689 (1) (1982) 1–11.
[62] S. Leavitt, E. Freire, Direct measurement of protein binding energetics by isothermal titration calorimetry, Curr. Opin. Struc. Biol. 11 (5) (2001) 560–566.